KFUPM
Journal of Undergraduate Research International

Diamond Open Access 8

Article Chemical Engineering

Cost-Effective $MnCo_2O_4/Co_2V_2O_7$ Mixed Oxide Electrocatalyst for Efficient Electrooxidation of 5-Hydroxymethylfurfural to 2,5-Furandicarboxylic Acid

Talal Mansour Al-Qahtani and Wasif Farooq*

Cite https://doi.org/10.64589/juri/231625

Submitted: April 25, 2026 **Revised:** May 17, 2026 **Accepted:** July 09, 2026

ABSTRACT

The intensive consumption of petrochemical-based products such as polyethylene terephthalate (PET) has adverse effects on the environment and public health. Consequently, the demand for bio-based alternatives has intensified. 5-Hydroxymethylfurfural (HMF) can be electrochemically oxidized to yield 2,5-furandicarboxylic acid (FDCA), a green plastic precursor. Despite the widespread use of noble-metal electrocatalysts for HMF oxidation, it still imposes major limitations such as high cost and limited scalability. This study investigated biomass valorization using a novel electrocatalyst for the electrooxidation of HMF to FDCA. $MnCo_2O_4/Co_2V_2O_7$ was synthesized via hydrothermal treatment followed by annealing. The composite material was comprehensively characterized using X-ray diffraction, scanning electron microscopy, electron-dispersive spectroscopy, and transmission electron microscopy. Electrochemical performance was evaluated using linear sweep voltammetry, cyclic voltammetry, electrochemical impedance spectroscopy, and Tafel slope analysis. $MnCo_2O_4/Co_2V_2O_7$ showed an onset potential of 1.44 V vs. the reversible hydrogen electrode for the HMF oxidation reaction (HMFOR), which was significantly lower than that for the oxygen evolution reaction (OER). Additionally, the catalyst demonstrated faster kinetics for HMFOR than for OER, as indicated by Tafel slopes of 104 mV dec^{-1} and 170 mV dec^{-1}, respectively. These results highlight the potential of $MnCo_2O_4/Co_2V_2O_7$, with multiple active sites provided by Mn, Co, and V, as a cost-effective electrocatalyst for the sustainable and scalable electrooxidation of HMF to FDCA.

Keywords: biomass valorization, Mn–Co–V mixed oxides, HMF electrooxidation, FDCA, bimetallic oxides

1. INTRODUCTION

Conventional production of petrochemical products, such as plastics, contributes to water and air pollution, as well as greenhouse gas emissions[1]. Bio-based materials have thus garnered considerable interest to reduce the reliance on fossil fuels and mitigate the carbon footprint. Notably, the electrochemical oxidation of biomass-derived platform molecules has emerged as a promising strategy for sustainable chemical production, combining renewable feedstocks with clean electrical energy. Renewable biomass resources, such as livestock waste and wood chips, represent promising substitutes for large-scale chemical production[2]. Lignocellulosic biomass, composed of cellulose, hemicellulose, and lignin, is especially attractive owing to its abundance, biodegradability, and the ability to be transformed into various value-added chemicals[3].

Among biomass-derived platform molecules, 5-hydroxymethylfurfural (HMF) has emerged as a promising precursor for bio-based polymer synthesis, as it can be obtained through the dehydration of C_6 and C_7 sugars derived from lignocellulosic materials[4]. The selective oxidation of HMF yields 2,5-furandicarboxylic acid (FDCA), a key monomer for synthesizing poly(ethylene furanoate) (PEF). Compared with conventional poly(ethylene terephthalate) (PET), PEF can reduce carbon emissions by approximately 70%, highlighting its potential as a sustainable polymer alternative. Given its industrial relevance, FDCA has been identified by the U.S. Department of Energy as one of the most valuable bio-based chemicals[5].

Electrochemical oxidation offers a green route for converting HMF to FDCA, and the use of an electrocatalyst has been noted to reduce the required potential to less than 1 V versus the reversible hydrogen electrode (RHE)[6]. Consequently, numerous studies have investigated noble metals (e.g., Pt, Au, Ag, and Ru) and their alloys as electrocatalysts for HMF electrooxidation. However, the use of noble metals is hindered by low current densities and FDCA yield. For example, Pt and Au exhibit low current densities in alkaline solutions (pH >13), whereas Ru displays lower current density than that achieved by Pt in acidic electrolytes[7–9]. Furthermore, monometallic electrodes such as Pd, Au, and Pt offer FDCA yields of less than 5% in HMF electrooxidation[10,11]. Overall, noble metals limit industrial scale-up owing to their high cost and poor catalytic performance[12]. To reduce costs, non-noble electrocatalysts have attracted considerable attention. Among these, transition metal oxides have been widely

Published under an exclusive license by KFUPM

explored as their diverse electronic configurations result in high electrocatalytic efficiency[13]. In particular, the integration of V-, Co-, and Mn-based oxides as bimetallic oxides can enhance electrocatalytic performance. For example, $Co_3O_4/Mn_{0.2}Co$ has been reported to achieve nearly 100% FDCA yields[13]. Nickel–cobalt oxide nanowires ($NiCo_2O_4$) achieved 90% FDCA yields with an onset potential of 1.35 V vs. RHE, indicating that Co-rich frameworks can considerably reduce the onset potential[14,15]. CuO–V_2O catalysts supported on Ni foam achieved FDCA yields of 95.96% with a Faradaic efficiency of 94.61%. Ni–V layered double hydroxides exhibited a current density of approximately 30 mA cm^{-2} at 350 mV under alkaline water oxidation conditions, nearly twice that of the corresponding Ni–Fe double hydroxide[16,17]. These studies highlight the potential of V-based oxides as effective electrocatalysts owing to their multiple oxidation states[18]. In addition, δ-MnO_2 has been noted to achieve a high FDCA yield and Faradaic efficiency of 98%, with an onset potential of 1.35 V vs. RHE. Mn-based oxides exhibit high stability in both acidic and alkaline electrolytes[19].

Previous reported catalysts, such as $Co_3O_4/Mn_{0.2}Co$ and $NiCo_2O_4$, primarily rely on one or two redox-active centers. In contrast, this study focused on $MnCo_2O_4$/Co2V2O7, combining Co, Mn, and V within a dual-phase oxide structure. The proposed framework leverages the advantages of Co^{2+}/Co^{3+} (surface oxidation), $Mn^{2+}/Mn^{3+}/Mn^{4+}$ (redox efficiency), and V^{4+}/V^{5+} (oxygen transfer). To the best of our knowledge, such a ternary architecture has not been previously considered for the HMF oxidation reaction (HMFOR). Moreover, hydrothermal synthesis followed by calcination under an H_2/Ar atmosphere provides a promising route to a stable, crystalline, and uniformly distributed bimetallic oxide catalyst supported on Ni foam (NF), offering a cost-effective and scalable alternative to noble-metal catalysts.

The objective of this study was to develop an efficient, non-precious electrocatalyst for biomass upgrading. A Mn–Co–V mixed oxide was synthesized through hydrothermal treatment followed by calcination. Its catalytic performance in the oxidation of HMF to FDCA was evaluated via electrochemical measurements, including linear sweep voltammetry (LSV) and cyclic voltammetry (CV), electrochemical impedance spectroscopy (EIS), and Tafel analysis. We hypothesized that Mn–Co–V mixed oxides exhibit reduced onset potentials (below 1.5 V vs. RHE for HMFOR and below 1.7 V vs. RHE for the oxygen evolution reaction (OER)). Additionally, it displayed faster kinetics for HMFOR than for OER, as indicated by Tafel slopes of 120 mV dec^{-1} and 190 mV dec^{-1}, respectively, and lower charge-transfer resistance for HMFOR. This work aims to enable cheaper, more scalable HMFOR synthesis for green plastic (PEF) production. The rest of this paper is structured as follows: Methodology describes the synthesis and characterization process; Results and Discussion discuss the structural and electrochemical results; Conclusions summarize the key results and future.

2. METHODOLOGY

2.1. Materials. HMF (99% purity) was purchased from Sigma-Aldrich in St. Louis, Missouri, USA. cobalt nitrate hexahydrate ($Co(NO_3)_2.6H_2O$; 99% purity) was obtained from AnalaR in Lutterworth, UK, ammonium metavanadate (NH_4VO_3; 95% purity) was purchased from BDH in Poole, UK, and manganese nitrate tetrahydrate ($Mn(NO_3)_2.4H_2O$; 98% purity) was obtained from Alfa Aesar in Ward Hill, Massachusetts, USA . Urea ($CO(NH_2)_2$) and ammonium fluoride (NH_4F; 95% purity) were obtained from Sigma-Aldrich. Deionized water (DI) and hydrochloric acid (HCl; 95% purity), ethanol (C_2H_5OH; 99.5% purity), commercial nickel foam (NF; 1 cm ×2 cm size), and potassium hydroxide (KOH; 85% purity) were purchased from Sigma-Aldrich.

2.2. Synthesis. A solution of 1 mmol of NH_4VO_3, 10 mmol of $CO(NH_2)_2$, and 4 mmol of NH_4F was dissolved in 30 mL of DI and magnetically stirred at 60 °C for 25 min. Subsequently, 1.5 mmol of $Mn(NO_3)_2.4H_2O$ and 1 mmol of $Co(NO_3)_2.6H_2O$ were introduced to obtain a solution with a Mn:Co:V molar ratio of 1.5:1:1. The mixture was stirred for an additional 10 min, poured into a stainless-steel autoclave reactor, and subjected to hydrothermal treatment at 140 °C for 12 h. Next, the solution was centrifuged and washed multiple times with water and ethanol for 15 min each. The product was then dried at 60 °C for 12 h, followed by annealing at 550 °C for 3 h in a 10% H_2/90% Ar atmosphere.

2.3. Electrode Fabrication. NF (1 cm × 2 cm) was immersed in 5–10 mL of 1 M HCl and sonicated for 15 min; the solution was then discarded. The sonication process was repeated using water and ethanol. The NF was then dried in an oven at 60 °C for 15 min. Next, 10 mg of the catalyst was added to a mixture of 1.4 mL of water and 0.6 mL of ethanol to prepare the catalyst ink. The solution was sonicated for 30 min. Subsequently, 300 µL of the resulting ink was drop-cast onto the NF and dried at 60 °C for 1 h. Figure 1 illustrates the methodology for synthesizing the Mn–Co–V oxide and fabricating the electrode.

2.4. Characterization. The crystalline structures of the synthesized catalysts were analyzed by X-ray diffraction (XRD) using a Rigaku MiniFlex diffractometer (Japan) operating at 40 kV and 15 mA with Cu Kα radiation ($\lambda = 1.5406$ Å). The surface morphology was observed using field-emission scanning electron microscopy (FESEM; TESCAN MIRA3), while the elemental composition was determined via energy-dispersive X-ray spectroscopy (EDS; INCA Energy 200, Oxford Instruments, UK). To enhance imaging resolution, the samples were coated with a ~10 nm Au layer prior to FESEM analysis. Transmission electron microscopy (TEM) was performed using a JEOL JEM-2100F at 300 kV.

2.5. Electrochemical Measurements. Electrochemical data were collected employing a Gamry Interface 1010 potentiostat/galvanostat (Gamry Instruments, Warminster, PA, USA). A three-electrode system was used to obtain electrochemical measurements for the HMFOR and OER. The working electrode, composed of $MnCo_2O_4/Co_2V_2O_7$, was cast onto an NF substrate with an active area of 1 cm^2. The reference electrode was an Hg/HgO electrode, and Pt wire was applied as the counter electrode. The electrolyte consisted of 1 M KOH with a pH of ≈13.67. Potentials collected from Hg/HgO were converted to the RHE scale using the following equation:

$$E_{RHE} = E_{Hg/HgO} + 0.059 \times (pH) + 0.105V \quad (1)$$

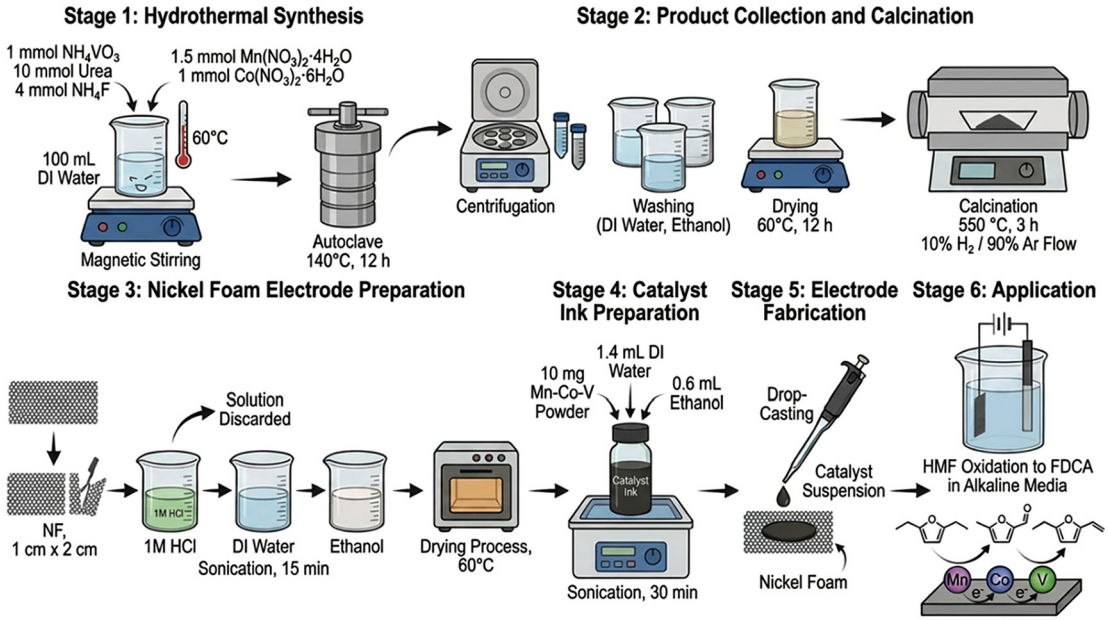


Figure 1. Schematic of the synthesis and electrode fabrication process for the (MnCo2O4/Co2V2O7)/NF electrocatalyst. Mn, Co, and V precursors are dissolved in deionized water, followed by hydrothermal treatment at 140 °C for 12 h. The product is calcined at 550 °C for 3 h under a 10% H2/90% Ar atmosphere to form the mixed metal oxide phase. Catalyst ink is then drop-cast onto nickel foam (NF) to prepare the working electrode for HMF electrooxidation

where E_{RHE} is the potential converted to the reversible hydrogen electrode scale, $E_{Hg/HgO}$ is the measured potential versus the Hg/HgO reference electrode.CV measurements were performed in 30 mL of 1 M KOH for 35 cycles over a potential range of 0–0.8 V vs. Eref at a scan rate of 50 mV s^{-1}. LSV was performed in 30 mL of 1 M KOH, with and without HMF. The Tafel slope was obtained from LSV measurements as

$$\eta = b \times \log(j) + a \tag{2}$$

where η is the overpotential, j is the current density, and b is the Tafel slope .and a is the Tafel equation intercept.

Electrochemical impedance spectroscopy (EIS) was performed over a wide frequency range of 10^{-1} Hz to 10^{5} Hz with a 1 cm^2 active area.

3. RESULTS AND DISCUSSION

3.1. Catalyst Characterization. The phase and crystallinity of the Mn–Co–V-based catalyst were examined by XRD (Figure 2). The diffraction pattern of the synthesized catalyst exhibits sharp peaks, indicating high crystallinity. Moreover, the peaks are consistent with the standard reference patterns for $MnCo_2O_4$ (JCPDS No. 00-023-1237) and $Co_2V_2O_7$ (JCPDS No. 01-070-1189)[20,21]. Specifically, the diffraction peaks at 36°, 54°, 63°, and 67°correspond to $MnCo_2O_4$, whereas those in the 23°–45°range (near 35°, 38°, 40.5°, and 43°) are ascribed to $Co_2V_2O_7$.

TEM images (Figure 3 (a) and (b)) reveal that the nanoparticles tend to aggregate, as commonly observed in metal oxides, facilitating electron transfer. Figure 3 (c) shows clear lattice fringes, indicating the highly crystalline or polycrystalline structure of the synthesized electrocatalyst, and Figure 3 (d) confirms its polycrystalline structure. As shown in Figure 3 (e)–(g), spherical particles are decorated on cube-like particles, confirming a homogeneous distribution of Co, Mn, and V throughout the catalyst, which is further proven by EDS mapping (Figure 3 (h) and (i)).

The average crystallite size is determined using the Scherrer equation:

$$D = \frac{K\lambda}{\beta\cos(\theta)} \tag{3}$$

Where D is the average crystallite size, $K = 0.94$, $\lambda = 0.15406$ nm, and β is the full width at half maximum (in radians). The average crystallite sizes were 43.7 nm for $MnCo_2O_4$ and 34.1 nm for Co2V2O7, resulting in an overall average crystallite size of 39.6 nm, consistent with the nanoparticulate morphology observed in the TEM images.

3.2. Electrochemical Performance. As shown in Figure 4 (b), the electrooxidation of HMF to FDCA involves the transfer of six electrons and can proceed through two routes. The anodic reaction in an alkaline electrolyte (like KOH) is presented in Eq. (1). In the first path, the alcohol group on HMF is oxidized to an aldehyde, forming 2,5-diformylfuran. Subsequently, the aldehyde is oxidized to a carboxylic group, forming 5-formyl-2-furancarboxylic acid (FFCA). In the second pathway, the aldehyde group in HMF is oxidized to form 5-hydroxymethyl-2-furancarboxylic acid (HMFCA) and then FFCA. Oxidation of the remaining aldehydes in FFCA ultimately yields FDCA.

The electrocatalytic performance of the as-prepared $MnCo_2O_4/Co_2V_2O_7$ catalyst was evaluated using CV, LSV, and EIS. OER and HMFOR kinetics were assessed in 1 M KOH, with and without 10 mM HMF, respectively. Figure 5 (a) shows the LSV curves for OER and HMFOR. Potentials close to 1.42 V

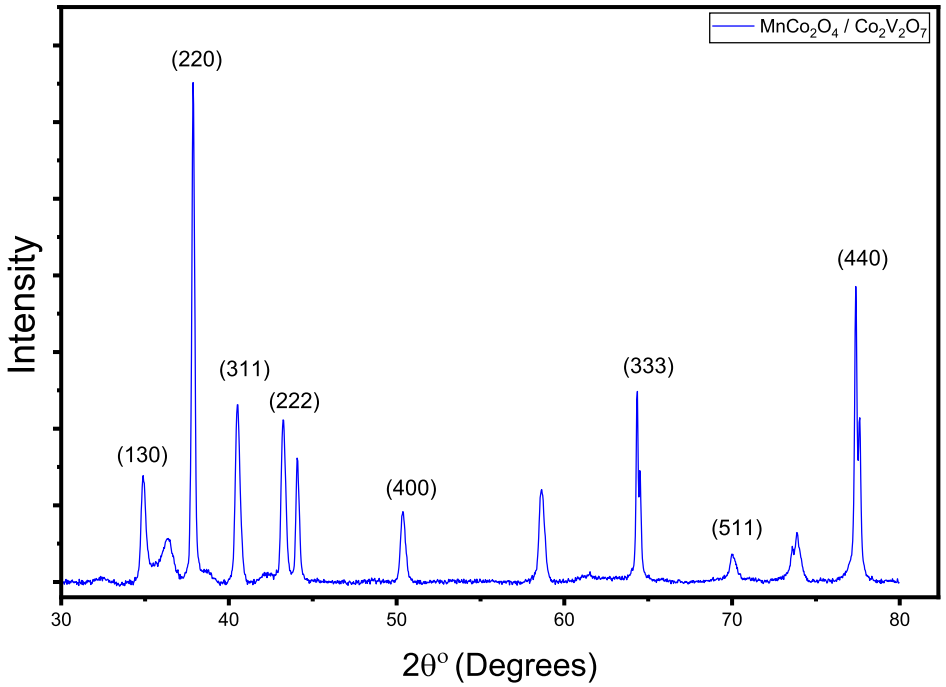


Figure 2. XRD pattern of ($MnCo_2O_4/Co_2V_2O_7$)/NF, along with Miller indices of the characteristic peaks The diffraction peaks correspond well with the reference patterns for MnCo2O4 (JCPDS No. 00-023-1237) and Co2V2O7 (JCPDS No. 01-070-1189), demonstrating the flourishing appearance of the bimetallic oxide phases and the lack of observable impurity peaks

are attributable to the oxidation of NF from Ni^{2+} to Ni^{3+}, with possible contribution from cobalt oxidation below this voltage. Therefore, the ($MnCo_2O_4$ /$Co_2V_2O_7$)/NF catalyst exhibits superior activity in the HMFOR (onset potential of 1.44 V vs. RHE) compared with the OER (1.6 V vs. RHE), demonstrating its effectiveness in biomass upgrading. This superior HMFOR performance is attributed to the active sites of Co, Mn, and V.

Figure 5 (b) shows the corresponding Tafel plots, based on LSV measurements. The HMFOR exhibits a Tafel slope of 104 mV dec^{-1}, lower than that of the OER (170 mV dec^{-1}). This indicates that ($MnCo_2O_4$ /$Co_2V_2O_7$)/NF exhibits faster reaction kinetics and more favorable electron transfer during the HMFOR.

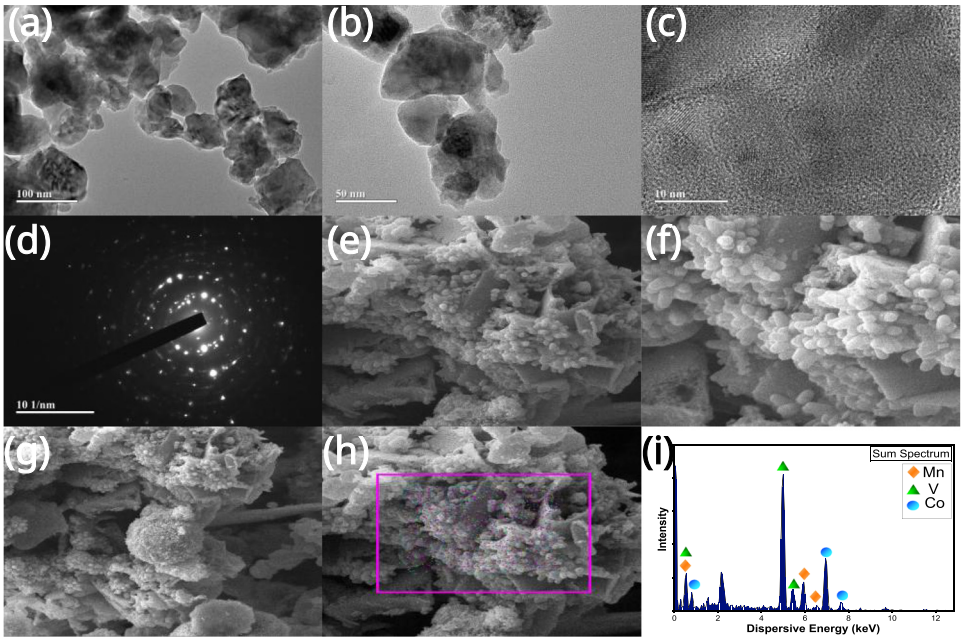


Figure 3. Characterization of the prepared catalyst: (a) TEM image (100 nm scale) demonstrating aggregated nanoparticles. (b) TEM image (50 nm). (c) TEM image (10 nm) illustrating nanocrystalline order. (d) SAED pattern confirming polycrystallinity. (e–g) SEM images at magnifications of 10, 20, and 4 kx, respectively.(h) EDS elemental mapping showing the uniform distribution of Mn (yellow), Co (cyan), and V (pink). (i) EDS spectrum, excluding oxygen for graph clearance

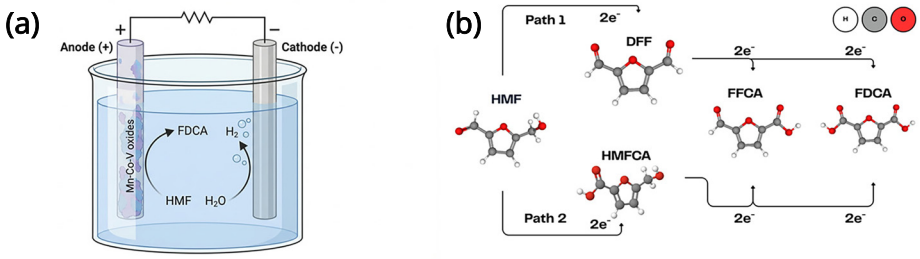


Figure 4. Schematic of electrochemical cell for the electrooxidation of HMF to FDCA using $(MnCo_2O_4/Co_2V_2O_7)$/NF as the catalyst. (b) Reaction pathways, involving the transfer of six electrons. Path 1 proceeds via DFF and FFCA intermediates; path 2 proceeds via HMFCA and FFCA intermediates

To further assess the electrocatalytic performance, CV was performed over the range of 1–1.8 V vs. RHE. As shown in Figure 5 (c), a clear peak appears at 1.3–1.45 V vs. RHE, corresponding to the oxidation of metal species, yielding active sites of Ni, Co, and Mn. A similar cathodic peak was observed in the reverse scan, corresponding to the coupled redox reaction of these metals. Furthermore, the CV curves showed a stable response over 35 cycles, indicating the electrochemical stability of the catalyst.

EIS was used to examine the resistance and kinetics during both the HMFOR and OER. The Nyquist plots are shown in Figure 5 (d). In general, a smaller semicircle diameter corresponds to lower charge-transfer resistance and faster interfacial electron-transfer kinetics. However, in this study, the HMFOR displays a larger semicircle than the OER. The low concentration of HMF in the alkaline solution likely enhanced resistance to the HMFOR, and the applied EIS voltage was below that required for the HMFOR. Thus, these results must be considered alongside the prior analyses, which highlight the more favorable kinetics of HMFOR.

Chronoamperometry (CA) was performed to assess the stability of the catalyst over one hour at a constant potential of 0.5 V vs. Eref. Figure 6 shows the current density of the $(MnCo_2O_4/Co_2V_2O_7)$/NF catalyst. The current density decreases slightly over time, indicating that HMF was converted into valuable chemicals. The enhanced HMFOR performance of $MnCo_2O_4/Co_2V_2O_7$ is likely attributable to the synergistic actions of the three metal centers. The elevated redox transitions of Co^{2+}/Co^{3+} produce high-valency cobalt–oxo species that occupy the central sites for the oxidation of HMF. The Mn^{2+}/Mn^{3+} pair introduces additional redox-active centers, facilitating the multi-electron transfer required for the subsequent oxidation of HMF intermediates. V also serves as an oxygen-transfer medium and stabilizes the reaction intermediates

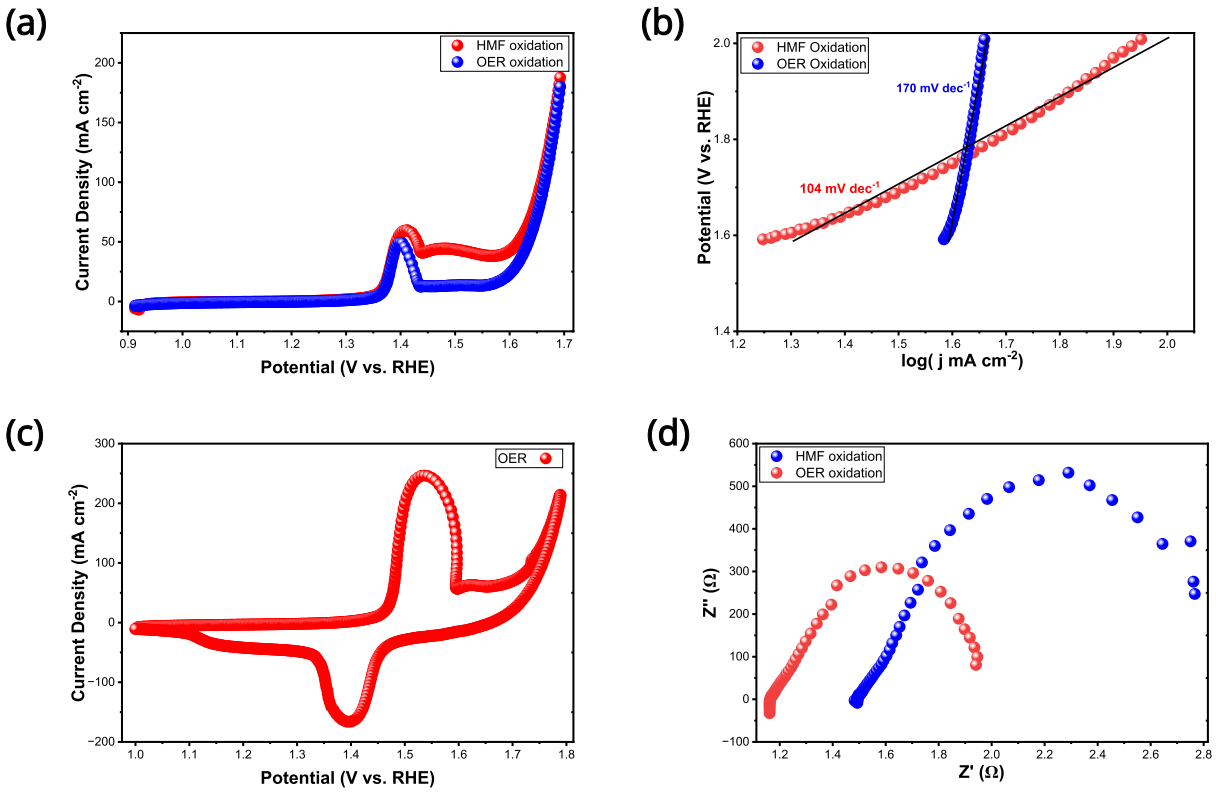


Figure 5. Electrochemical performance: (a) LSV curves for HMFOR and OER. (b)Tafel plots derived from LSV data. (c) CV curves over 35 cycles. (d) Nyquist plots derived from EIS measurements

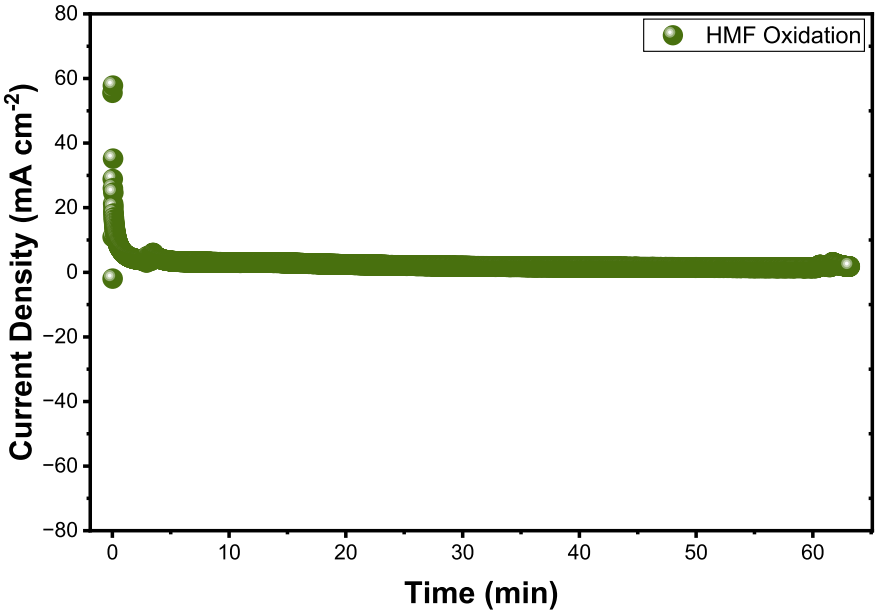


Figure 6. CA measurements conducted for 1 h at 0.5 V vs. Eref for HMFOR

HMFCA and FFCA through V^{4+}/V^{5+} cycling, enabling complete oxidation to FDCA.

4. CONCLUSIONS

A Mn–Co–V metal-oxide catalyst was synthesized via hydrothermal treatment followed by calcination under a 10% H_2/90% Ar atmosphere. The Mn–Co–V metal-oxide catalyst were used as non-precious anodes for the oxidation of HMF to FDCA. XRD analysis confirmed that the catalyst matched the crystal structures of $MnCo_2O_4$ (JCPDS No, 00-023-1237) and $Co_2V_2O_7$ (JCPDS No. 01-070-1189), with uniform distributions of Mn, Co, and V. LSV tests showed that the catalyst demonstrated superior performance toward the HMFOR, with an onset potential at 1.44 V vs. RHE, lower than that for the OER (1.6 V). In addition, more favorable kinetics were noted for the HMFOR, with a Tafel slope of 104 mV dec^{-1}, lower than that for the OER (170 mV dec^{-1}). EIS analysis indicated a limitation at low HMF concentrations, as reflected by the larger semicircles in the Nyquist plot and the low applied voltage during the experiments. Overall, the)$MnCo_2O_4$ /$Co_2V_2O_7$(/NF catalyst offers a green and cost-effective approach for scaling FDCA production. Its enhanced performance is ascribed to the redox conjunctional capability of Co^{2+}/Co^{3+}, Mn^{2+}/Mn^{3+}, and V^{4+}/V^{5+} pairs, which act as multi-electron transfer channels and intermediate stabilizers for the stepwise oxidation of HMF toward FDCA. This unlocks the potential to scale the green plastic industry, such as PEF, which can be produced from FDCA monomers. This article imposes some limitations such as FDCA yield experiment and EIS results which will be added in future work.

AFFILIATIONS AND AUTHOR DETAILS

Undergraduate Authors

Talal Mansour Al-Qahtani – *Chemical Engineering Department, King Fahd University of Petroleum & Minerals, Dhahran 31261, Saudi Arabia*; 0009-0001-5718-4395
Email: s202153610@kfupm.edu.sa

Corresponding Author

Wasif Farooq – *Research Mentor, Associate Professor, Chemical Engineering Department, King Fahd University of Petroleum & Minerals, Dhahran 31261, Saudi Arabia*; 0000-0002-4882-0097
Email: wasif@kfupm.edu.sa

ACKNOWLEDGEMENTS

The authors would like to acknowledge the support provided by the Department of Engineering and the Interdisciplinary Research Center at King Fahd University of Petroleum and Minerals. This research was funded by the under project no. SMPL-ENG-2025-123. The authors also declare that they have no known competing financial or personal interest to influence this work presented in the article.

REFERENCES

(1) Wei, S. *et al.* Advances in the research of 2,5-furandicarboxylic acid (FDCA)-based polymers. *European Polymer Journal* vol. 241 Preprint at https://doi.org/10.1016/j.eurpolymj.2025.114364 (2025).

(2) Wang, C., Zhang, L., Zhou, T., Chen, J. & Xu, F. Synergy of Lewis and Brønsted acids on catalytic hydrothermal decomposition of carbohydrates and corncob acid hydrolysis residues to 5-hydroxymethylfurfural. *Sci. Rep.* **7**, (2017).

(3) Kamdem Tamo, A. *et al.* Lignocellulosic biomass and its main structural polymers as sustainable materials for (bio)sensing applications. *Journal of Materials Chemistry A* vol. 13 24185–24253 Preprint at https://doi.org/10.1039/d5ta02900g (2025).

(4) Mittal, A., Pilath, H. M. & Johnson, D. K. Direct Conversion of Biomass Carbohydrates to Platform Chemicals: 5-Hydroxymethylfurfural (HMF) and Furfural. *Energy and Fuels* **34**, 3284–3293 (2020).

(5) Marshall, A., Jiang, B., Gauvin, R. M. & Thomas, C. M. 2,5-Furandicarboxylic Acid: An Intriguing Precursor for Monomer and Polymer Synthesis. *Molecules* vol. 27 Preprint at https://doi.org/10.3390/molecules27134071 (2022).

(6) Pei, A. *et al.* Enhanced electrocatalytic biomass oxidation at low voltage by Ni2+-O-Pd interfaces. *Nat. Commun.* **15**, (2024).

(7) Latsuzbaia, R. *et al.* Continuous electrochemical oxidation of biomass derived 5-(hydroxymethyl)furfural into 2,5-furandicarboxylic acid. *J. Appl. Electrochem.* **48**, 611–626 (2018).

(8) Cao, T. *et al.* Selective Electrogenerative Oxidation of 5-Hydroxymethylfurfural to 2,5-Furandialdehyde. *ChemSusChem* **10**, 4851–4854 (2017).

(9) Heidary, N. & Kornienko, N. Operando Raman probing of electrocatalytic biomass oxidation on gold nanoparticle surfaces. *Chemical Communications* **55**, 11996–11999 (2019).

(10) Park, M., Gu, M. & Kim, B. S. Tailorable Electrocatalytic 5-Hydroxymethylfurfural Oxidation and H2Production: Architecture-Performance Relationship in Bifunctional Multilayer Electrodes. *ACS Nano* **14**, 6812–6822 (2020).

(11) Vuyyuru, K. R. & Strasser, P. Oxidation of biomass derived 5-hydroxymethylfurfural using heterogeneous and electrochemical catalysis. *Catal. Today* **195**, 144–154 (2012).

(12) Ma, Z., Wang, L., Li, G. & Song, T. Recent Advances in Electrocatalytic Oxidation of 5-Hydroxymethylfurfural to 2,5-Furandicarboxylic Acid by Heterogeneous Catalysts. *Catalysts* vol. 14 Preprint at https://doi.org/10.3390/catal14020157 (2024).

(13) Gao, T., Yin, Y., Zhu, G., Cao, Q. & Fang, W. Co3O4 NPs decorated Mn-Co-O solid solution as highly selective catalyst for aerobic base-free oxidation of 5-HMF to 2,5-FDCA in water. *Catalysis Today* vol. 355 252–262 Preprint at https://doi.org/10.1016/j.cattod.2019.03.065 (2020).

(14) Cheng, C. *et al.* High-efficiency bifunctional electrocatalyst based on 3D freestanding Cu foam in situ armored CoNi alloy nanosheet arrays for overall water splitting. *J. Power Sources* **427**, 184–193 (2019).

(15) Gao, L. *et al.* Hierarchical Nickel–Cobalt-Based Transition Metal Oxide Catalysts for the Electrochemical Conversion of Biomass into Valuable Chemicals. *ChemSusChem* **11**, 2547–2553 (2018).

(16) Xie, Z. *et al.* Boosting Biomass Electrooxidation using Synergistic Copper Vanadium Catalytic Interfaces. https://doi.org/10.2139/ssrn.6020399 (2026) doi:10.2139/ssrn.6020399.

(17) Fan, K. *et al.* Nickel-vanadium monolayer double hydroxide for efficient electrochemical water oxidation. *Nat. Commun.* **7**, (2016).

(18) Langeslay, R. R. *et al.* Catalytic Applications of Vanadium: A Mechanistic Perspective. *Chemical Reviews* vol. 119 2128–2191 Preprint at https://doi.org/10.1021/acs.chemrev.8b00245 (2019).

(19) Wang, C., Bongard, H. J., Weidenthaler, C., Wu, Y. & Schüth, F. Design and Application of a High-Surface-Area Mesoporous δ-MnO2Electrocatalyst for Biomass Oxidative Valorization. *Chemistry of Materials* **34**, 3123–3132 (2022).

(20) Oroumi, G., Samimi, F., Mahdi, M. A., Dawi, E. A. & Salavati-Niasari, M. Insights into the photocatalytic role of glycine-assisted sol-gel auto-combustion synthesized (Co, Mn)(Co, Mn)$_2$O$_4$ nanostructures for efficient visible light-driven degradation of methyl orange. *Arabian Journal of Chemistry* **17**, (2024).

(21) Chu, X. *et al.* Hard-Template-engaged formation of Co2V2O7 hollow prisms for lithium ion batteries. *RSC Adv.* **8**, 2072–2076 (2018).